Single-shot reconstruction of the density profile of a dense atomic gas

C. Mordini[1], D. Trypogeorgos[1, 2, *], L. Wolswijk[1], G. Lamporesi[1, 2], and G. Ferrari[1, 2]

[1] *INO-CNR BEC Center and Dipartimento di Fisica, Università di Trento, 38123 Povo, Italy*
[2] *Trento Institute for Fundamental Physics and Applications, INFN, 38123 Povo, Italy*
[*] d.trypogeorgos@unitn.it
http://bec.science.unitn.it/

Abstract: Partial transfer absorption imaging (PTAI) of ultracold atoms allows for repeated and minimally-destructive measurements of an atomic ensemble. Here, we present a reconstruction technique based on PTAI that can be used to piece together the non-uniform spatial profile of high-density atomic samples using multiple measurements. We achieved a thirty-fold increase of the effective dynamic range of our imaging, and were able to image otherwise saturated samples with unprecedented accuracy of both low- and high-density features.

1. Introduction

Resonant absorption imaging (RAI), a broadly employed method for imaging cold atomic samples, measures the transmission of the atomic medium, which scales exponentially with the optical density (OD). Atomic ensembles near/past the Bose-Einstein condensation (BEC) threshold can have extremely high peak densities $n_0 \gtrsim 10^{20}\,\mathrm{m}^{-3}$, which translates to typical peak ODs $\gtrsim 100$, way past the saturation limit of RAI [1]. Although for large BECs this problem persists even when imaging an expanded and dilute cloud, it is exacerbated for direct in-situ imaging [1]. Even in regimes of saturated absorption and high-intensity imaging [2, 3], the dynamic range of RAI allows access to a range of ODs of no more than an order of magnitude. Moreover, the process is fully destructive, since it imparts large kinetic energy to the BEC, and it allows for a single image per experiment; its use for measuring dynamic processes is limited by the cycle-time of the experiment, which is typically a few tens of seconds, and is only applicable in case of fully reproducible events.

Alternative imaging methods, such as phase-contrast [4, 5], Faraday imaging [6, 7], and diffraction contrast imaging [8], take advantage of the high index of refraction of the BEC and give a dispersive signal. Although these techniques are non-destructive, their dynamic range is still limited in a manner similar to RAI.

Here, we demonstrate a technique, based on partial transfer absorption imaging (PTAI) [9], that is capable of minimally-destructive imaging and has an exceedingly larger dynamic range. PTAI is a versatile method that was used for in-situ imaging of superfluid flow in annular geometries [10, 11], to observe the real-time dynamics of vortices [12–14], in-trap oscillations of a quantum gas [15], and measurement of the thermodynamic equation of state of an atomic gas [16]. It is implemented by coherently transferring a fraction of the atoms to an auxiliary energy level where it can be imaged by means of an optical cycling transition to an electronically excited state (Fig. 1b). The non-transferred atoms remain in the ground level which is far off-resonance from the optical transition and are left largely undisturbed by the imaging light.

Our technique accurately measures the in-situ density profile of condensed samples by taking several partial-transfer pictures, tuning the fraction of the outcoupled atoms so as to image areas of the BEC in different ranges of atomic densities, always with optimum signal-to-noise ratio. A reconstruction algorithm we developed, similar to high-dynamic-range (HDR) photography [17],
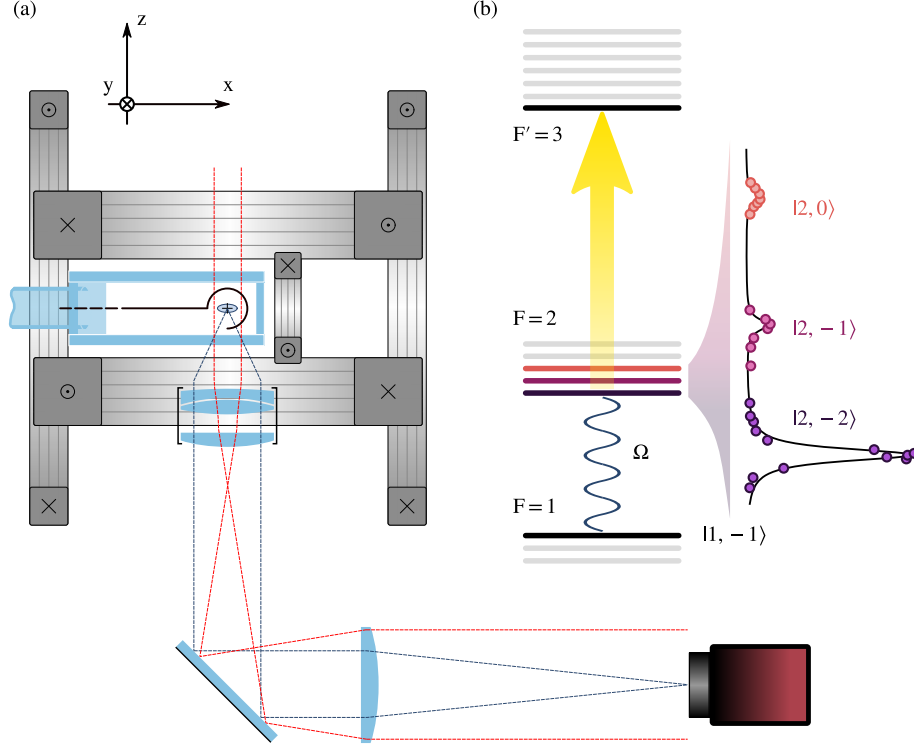
Fig. 1. Experimental apparatus and atomic transitions. (a) The BEC (blue) is confined by the magnetic field generated by the five coils (gray). It is imaged in absorption along the z-axis using a relay optical system. The microwave field is generated by a hook antenna placed on the side of the glass cell. (b) The atoms, initially in $|1, -1\rangle$, are transferred via microwave radiation of Rabi frequency Ω to $|2, -2\rangle$ and are subsequently imaged in $F' = 3$. The spectroscopy (vertical) shows the three allowed microwave transitions between $|1, -1\rangle$ and the $F = 2$ manifold.

pieces together the information from different measurements allowing us to obtain a complete density profile of the trapped sample in a single shot. In this manner, our technique does not directly extend the dynamic range of RAI, but allows for it to be applied to atomic samples of arbitrary density.

2. Experiment

In our experiment we produce ^{23}Na BECs with about $N = 5 \times 10^6$ atoms. Our apparatus is described elsewhere [18]; here we focus only on the imaging part along the z-axis. The sample is trapped in a magnetic Ioffe-Pritchard trap with an elongated geometry with trapping frequencies $\omega_x/2\pi = 8.83(2)$ Hz, $\omega_y/2\pi = \omega_z/2\pi = 100.8(7)$ Hz, and is polarized in the $|F, m_F\rangle = |1, -1\rangle$ hyperfine ground level. A $|B| = 1$ G bias magnetic field is applied to the system along x, corresponding to a Larmor frequency of 700 kHz. We implement PTAI using a ≈ 1.77 GHz microwave field to transfer a fraction of the atoms to the upper hyperfine manifold $F = 2$, that we subsequently image with light resonant to the $F = 2 \rightarrow F' = 3$ cycling transition. The microwave

field is generated by a signal generator [1], amplified with a 100 W amplifier [2], and delivered to the atoms via a hook antenna (Fig. 1a).

The microwave-field coupling induces Rabi oscillations between the two levels and the fraction of atoms transferred after a pulse time t is

$$P(t, \delta) = \left(\frac{\Omega}{\tilde{\Omega}(\delta)}\right)^2 \sin^2\left(\frac{\tilde{\Omega}(\delta)\, t}{2}\right), \tag{1}$$

with Ω the Rabi frequency and δ the detuning from resonance that lead to the system oscillating at the generalised Rabi frequency $\tilde{\Omega} = \sqrt{\Omega^2 + \delta^2}$.

We use $|2, -2\rangle$ as an auxiliary state for the imaging, since this is the transition that has the largest Clebsch-Gordan coefficient, and spin-flipping collisions in the resulting hyperfine mixture are suppressed due to conservation of total angular momentum [19]. The choice of the auxiliary state is not crucial for the subsequent imaging, as the separation of the $F = 2$ magnetic sublevels is of the order of the precession frequency and much smaller than the optical linewidth of 10 MHz. Figure 1b shows the population of the individual magnetic sublevels in the $F = 2$ manifold with respect to the microwave frequency.

Finally, we image the atoms in-situ using a relay imaging system with a magnification of 8.0(1) and a resolution of 2 μm. The probe light along the z-axis is absorbed resonantly by the atoms in the upper hyperfine manifold and casts a shadow in the camera [3]. Combining the pictures with and without the atoms present, we reconstruct the OD of the sample from the ratio of the image counts (see Appendix A in [1]).

3. HDR reconstruction method

For these measurements we produce condensates at a temperature of about 230 nK, corresponding to a BEC fraction of about 50%. We image different regions of the condensed sample using a sequence of microwave pulses tuned to be sensitive to different density ranges. Short pulses transfer a small fraction of atoms, whose spatial distribution is the same one as the original BEC and in the center has a peak OD ≈ 4 which can be imaged reliably with high-intensity RAI. The OD in the thermal tails however, is still too low to be measured with a sufficient signal-to-noise ratio. Longer microwave pulses increase the apparent OD of the thermal part while the centre of the cloud becomes too optically thick saturating the imaging (Fig. 2).

Using a method inspired by HDR photography, we combine the information from different images to reconstruct a complete image of the column density of the trapped sample. We take a series of pictures with increasingly longer microwave pulses. On resonance, $\delta = 0$, the fraction of extracted atoms $P(t)$ is calculated from Eq. 1 using only the known Rabi frequency Ω. The inhomogeneous field of the magnetic trap introduces a spatial dependency in $P(t)$, that is negligible for $\Omega/2\pi > 20$ kHz (see Section 5.1). In each picture, we choose the extracted fraction in order to bring a different part of the cloud to a level of OD optimal for our imaging parameters, that are appropriate for dense ^{23}Na BECs [20].

We crop the regions in the pictures that are above the saturation threshold OD = 4, except for the smallest extraction where the peak OD is already below the threshold. We rescale each picture by the corresponding extraction fraction, and overlay them on top of each other. We then combine the data from all the pictures and average all of them, weighting them by the signal-to-noise ratio in the overlap regions, to get the reconstructed density.

Figure 2 shows a pictorial representation of the reconstruction method. In the top panel there is a stack of three different frames, imaged with increasing microwave pulsetimes (from

---

[1] Marconi Instruments 2024

[2] Minicircuits ZHL-100W-272+
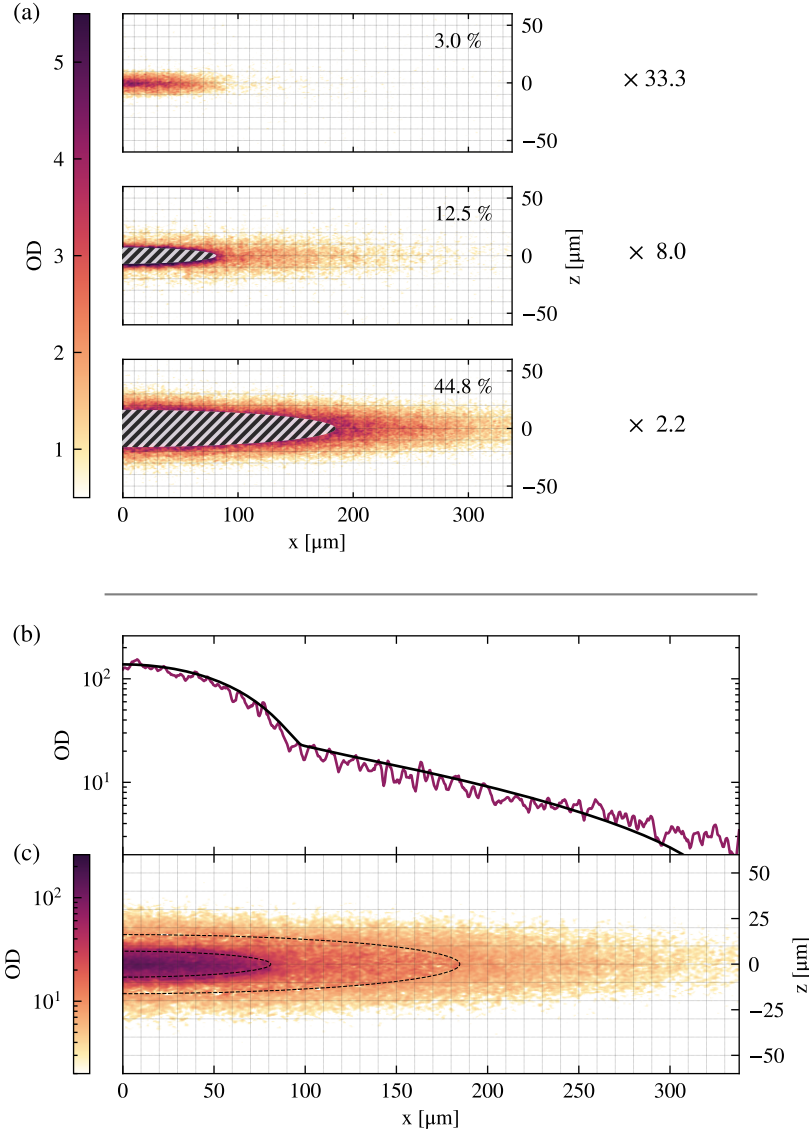
[3] Allied Vision Stingray F-201B

Fig. 2. Reconstruction method. (a) Three frames taken in a single shot are rescaled with the shown factors that are the inverse of the different extraction fractions. The grid size is roughly equal to five times our resolution. (b, c) The resulting HDR image is the weighted mean of the above frames. The dotted ellipses correspond to the cropped-out regions above. The profile of a one-dimensional slice at the center of the density profile agrees well with the Hartree–Fock theory (black line). Notice that the OD spans two orders of magnitude in the reconstructed image.
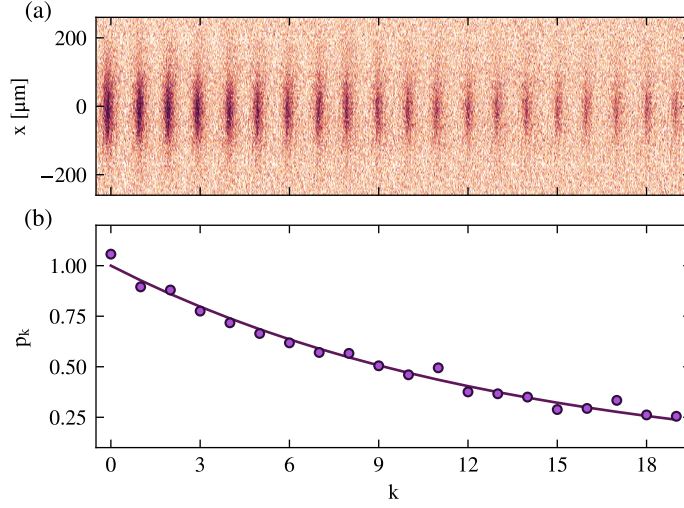
Fig. 3. Single-shot measurement of the Rabi frequency. (a) An image sequence showing the OD of the BEC after each partial extraction. A constant fraction of atoms is extracted every 16 ms. (b) The relative atom number progression is modelled with a geometric series (solid line) from which the value of the Rabi frequency can be calculated.

top to bottom) $0.9\,\mu s$, $1.94\,\mu s$, $4\,\mu s$, which for $\Omega/2\pi = 59.2(3)\,kHz$ correspond to extraction fractions 3%, 12.5%, 44.8% respectively; each picture is rescaled with the corresponding factor. The complete reconstruction of the atomic density is shown in Fig. 2c and corresponds to the weighted average of the rescaled pictures above. Along the long axis of the trap, we fit the OD to a Hartree–Fock profile [21] to verify that our reconstruction algorithm leads to physically meaningful results (see Fig. 2b).

4. Calibration of the Rabi frequency

The implementation of our HDR method requires the knowledge of Ω and δ, the only two parameters appearing in Eq. 1, to precisely determine the in-situ OD of the atomic sample. On resonance, $\delta = 0$, and the only remaining parameter is the Rabi frequency Ω which we obtain in a single shot using anew PTAI.

The Rabi frequency Ω can be measured by simply following the Rabi flopping of the system (see Fig. 4a). This is normally done by pulsing the coupling field for a given time t and then measuring both the ground- and excited state populations using a Stern-Gerlach technique to minimize errors in the Rabi frequency due to shot-to-shot number fluctuations in the preparation of the atomic sample. In our case, we implement this by letting the transferred atoms fall under the action of gravity and the antitrapping magnetic field. We image the falling atoms after a time-of-flight (TOF) of $\sim 10\,ms$ and the remaining atoms are then released from the trap and imaged in TOF with an optical repumper.

However, the dynamics of the system are actually governed by the generalised Rabi frequency $\tilde{\Omega}$. A non-uniform detuning (such as the one present in a magnetically trapped sample) leads to a locally varying precession rate which in practice reduces the spatial coherence of the oscillations (see Section 5.1). Maximising Ω allows us to partially circumvent this limitation by reducing the duration the coupling field is applied for. From Eq. 1 it follows that for $\tilde{\Omega}t \ll 1$ the transferred fraction $\tilde{\Omega}^2 t^2/2$ is independent of the microwave frequency. For a given product $\tilde{\Omega}t$, a large Rabi frequency reduces the distortions, as the detuning term $\delta \ll \Omega$ becomes negligible due to power-broadening of the resonance and the transfer fraction is now proportional to the Rabi

frequency Ω.

To this end we devised an alternative method to measure Ω which can also be done in a single-shot, dramatically increasing the measurement rate. We apply a sequence of microwave pulses coupling to $|2, -2\rangle$ to extract a small fraction of the trapped sample every 16 ms. We repeatedly image the extracted atoms after a 4 ms time-of-flight (TOF) using a camera along y (not shown in Fig. 1), for up to 20 times before the BEC is depleted, recording the atom number over time (see Fig. 3a). Applying always the same microwave pulse, the number of atoms in the cloud decreases by a constant fraction $q = \sin^2(\Omega t/2)$ at each extraction. With N_k the number of atoms extracted after $k + 1$ pulses, the relative number of extracted atoms $p_k = N_k/N_0$ follows a geometric series $p_k = (1 - q)^k$. From the series shown in Fig. 3b we obtain q, which leads to a Rabi frequency of 58.8(5) kHz for a $t = 1.5\,\mu$sec pulse, that is consistent with the value measured by following the Rabi flopping in multiple shots, with the advantage of being far less sensitive to the frequency detuning between the coupling field and the individual resonance of each atom. In fact this method allows to considerably reduce the duration of the pulses for the same intensity of the applied microwave field, hence suppressing the effects of the local detuning due to the Fourier spectral broadening of the applied pulse.

5. Considerations

5.1. Non-uniform magnetic field

The equilibrium position of the BEC does not coincide with the minimum of the magnetic field, due to the gravitational sag, $z_{sag} = g/\omega_z^2$, where g is the local acceleration of gravity. This leads to the detuning

$$\hbar\delta(x, y, z) = \frac{3}{2}m\left(\omega_x^2 x^2 + \omega_y^2 y^2 + \omega_z^2(z^2 - 2zz_{sag})\right) \tag{2}$$

varying quadratically along all directions, where m is the mass of ^{23}Na and the factor 3 corresponds to the Bohr magneton difference between the two coupled states, and the origin is centered on the BEC. Since the BEC experiences a non-uniform detuning, the transferred fraction varies locally, which introduces distortions in the measured density profile and prevents the transferred fraction from reaching unity. We modelled this effect (see Appendix A) and identified the parameter regime where it can be neglected for the measurement of in-situ density profiles.

We estimated the systematic error on the density measurement by computing the spatial dependency of $P(t, \delta)$ for our trap geometry, using Eq. 2. Typical Rabi oscillation measurements are shown in Fig. 4a and are of the order of a few tens of kHz. Figure 4b shows the spatial dependence of the transferred fraction in the xz plane centered at the position of the atoms, calculated for a reference extraction fraction of 20%. The atomic sample occupies an area delimited by the gray ellipses. Their semi-axes are equal to the Thomas–Fermi radii of the BEC (inner) and $2.5\,\sigma$, where σ is the width of the thermal cloud (outer). With the resonance fixed at the center of the atomic cloud, located at the axes origin, the non-uniformity is stronger along the z direction, due to the gravitational sag. A Rabi frequency of about 50 kHz allows to extract up to 15% of the sample with a top-to-bottom difference in the extraction at the edges of the BEC of less than 1%. The non-uniformity affects the extraction in the tails of the thermal cloud significantly more, with a top-to-bottom difference of up to 25%. However, the atomic density in those regions is 10^2 times smaller than in the BEC fraction, so that they have a negligible contribution to the integrated column density.

5.2. Collective mode excitation

The excitation of collective modes can potentially distort the reconstructed density profile of the BEC. The dipole mode, simply translates the BEC without distorting it; the BEC can be re-centered as long as the translation is perpendicular to the imaging axis but might otherwise
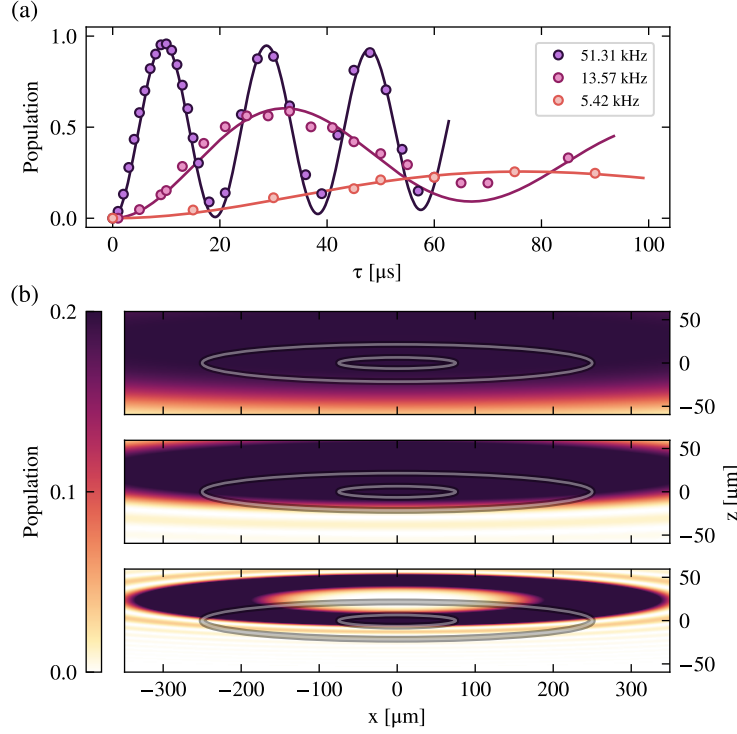
Fig. 4. Non-uniform Rabi flops. (a) The population of the upper state oscillates at less than full amplitude depending on the value of Ω due to the spatial dependence of δ. (b) Calculated spatial dependence of the extracted population fraction for the Rabi frequencies shown in (a), 51.31 kHz, 13.57 kHz, 5.42 kHz from top to bottom. The gray ellipses show the extent of the BEC (inner) and the thermal cloud (outer).

introduce focusing errors. Higher order modes, e.g. the quadrupole mode, are naturally excited during the extraction process [12] and distort the shape of the BEC at timescales close to the inverted trapping frequencies. It is possible to work around this effect by arranging for the sampling frequency to be equal to the mode frequency so all subsequent images are consistent with each other.

However, avoiding its excitation altogether is preferable. Moreover, if the sampling frequency is much faster than the mode frequency the shape of the BEC can be considered essentially frozen. Figure 5 shows the variations of the Thomas–Fermi radius along the x axis, R_x, normalised to its value before any extraction takes place, for different extraction fractions. The relative amplitude of the excited quadrupole mode ΔR_x is smaller than 0.05 for extractions smaller than 3.5%. Motivated by this observation, we arranged the sequence of images in Fig. 2 as follows. The 3.5% image is taken at $t = 0$ and leaves the BEC largely undisturbed. Then the 12.5% and 44.8% images are taken 70 ms later but only 600 μs apart, which is much smaller than the period of the quadrupole mode. Within these 600 μs we shine a 5 μs resonant pulse along y that pushes the atoms along a transverse direction thus removing them from the field of view.

5.3. Off-resonant scattering

Acquiring multiple measurements normally requires an equal number of atom-light interactions with the imaging laser resonant to the $F = 2 \rightarrow F' = 3$ transition. An imaging laser pulse follows
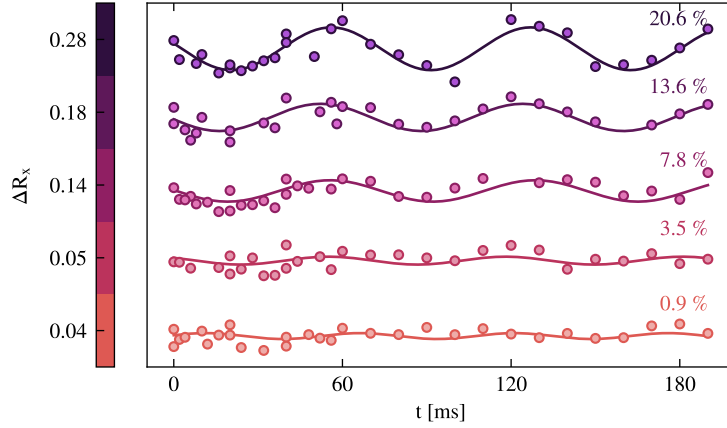
Fig. 5. Quadrupole mode excitation. The Thomas–Fermi radius oscillates in time after a single extraction has taken place. The oscillations for different extraction fractions are shifted vertically for clarity. The curves are coloured based on the relative value of their oscillation amplitude ΔR_x, which is directly proportional to the extraction fraction. The quadrupole mode becomes appreciable for extraction fractions larger than 5%.

the transfer of atoms from $F = 1 \rightarrow F = 2$. The laser light interacts off-resonantly with atoms in the otherwise shelved $F = 1$ state, which for ^{23}Na is 1.77 GHz detuned, and leads to the reservoir of atoms being depleted [22]. This introduces a systematic error in the measurement of the atom number for the subsequent images which can be measured and accounted for. For our typical imaging intensity $I/I_{sat} = 4$, where $I_{sat} = 13.4\,\text{mW/cm}^2$ is the saturation intensity of ^{23}Na, the off-resonant scattering rate is $10^3\,\text{s}^{-1}$, which leads to negligible losses for a 5 μs imaging pulse.

Incidentally, the non resonant scattering from $F = 1$ atoms also affects the apparent number count of $F = 2$ atoms for slightly out-of-focus systems [23].

6. Conclusions

We developed a powerful single-shot, HDR atomic imaging method which allows to increase the dynamic range of the imaging by more than one order of magnitude and accurately reconstruct the true OD of the atomic sample. The fraction imaged within each PTAI snapshot is optimized to different ranges of the OD, while the merging of the information from different snapshots is implemented thanks to the accurate knowledge of the extracted fraction. The final outcome is the complete column-integrated atomic density distribution. We also devised a procedure for measuring the Rabi frequency of the microwave transitions which is highly insensitive to non-uniformities across the atomic system. The method is based on the iterated application of short microwave pulses of constant duration and is benchmarked against usual Rabi flopping.

We expect our HDR reconstruction method to be widely applicable to a number of similarly dense atomic systems like quantum droplets [24–26]. We have already successfully used it to measure the equation of state of a three-dimensional bosonic gas [16].

Appendix A: Non-uniform Rabi model

After the application of a microwave pulse of time t, the transferred fraction to $F = 2$ is

$$\tilde{P}(t) = \frac{N_2}{N} = \frac{1}{N} \int P(t, \delta(r))\, n(r)\, d^3r, \tag{3}$$

where $N = N_1 + N_2$ is the total number of atoms. The probability distribution of Eq. 1 is weighted by the atomic density and spatially integrated.

To calculate the effective value of Ω via Rabi flopping, we introduce some approximations. Since the field variation along z is small with respect to the atomic cloud size, we retain only the linear term for the gravitational sag in Eq. 2 and rewrite $\delta \propto 2zz_{sag}$. We approximate the atomic density distribution with a Gaussian shape and integrate out the transverse spatial directions, where the detuning remains constant. Equation 3 now becomes

$$\tilde{P}(t) \simeq \frac{1}{\sqrt{2\pi}\Delta_0} \int P(t, \delta)\, e^{-\delta^2/2\Delta_0^2}\, d\delta, \tag{4}$$

which explicitly shows that the effect of the field gradient is to average the transferred population over the local detuning. Δ_0 is the detuning spanned by the condensate due to the varying magnetic field and depends on the microwave field strength and the size of the atomic sample. The contrast of the Rabi oscillations is reduced since the effective detuning varies across the cloud and atoms at different regions oscillate with slightly different generalised Rabi frequencies. Large Ω and small atomic samples reduce this effect and lead to Rabi oscillations with full contrast. In our trap, a BEC of 5×10^6 atoms has a transverse Thomas-Fermi radius of $12\,\mu m$, which corresponds to $\Delta_0 = 20\,kHz$.

Within these approximations the integral in Eq. 4 can be solved analytically and the result for the modified population transfer is

$$\tilde{P}(t) = \frac{1}{2\sqrt{1 + 2D^2}} \left(1 - \frac{\cos(\tau + \arctan(b)/2)}{(1 + b^2)^{1/4}} \right), \tag{5}$$

where $\tau = \Omega t$, $D = \Delta_0/\Omega$ and $b = \tau D^2/(1 + 2D^2)$.

To check the validity of this approximate model, we also computed the transferred fraction numerically from Eq. 3, using the detuning from Eq. 2, our trap parameters, and a Thomas–Fermi density distribution with the known number of atoms. We fitted the data in Fig. 4 to the numerically computed fraction with Ω as the only free parameter, and found that the analytical approximation agrees well with the numerical model.

Funding

References

1. W. Ketterle, D. S. Durfee, and D. M. Stamper-Kurn, "Making, probing and understanding Bose-Einstein condensates," in *Proc. Int. Sch. Phys. "Enrico Fermi"*, C. W. M. Inguscio, S. Stringari, ed. (1999).
2. G. Reinaudi, T. Lahaye, Z. Wang, and D. Guéry-Odelin, "Strong saturation absorption imaging of dense clouds of ultracold atoms," Opt. Lett. **32**, 3143 (2007).
3. K. Hueck, N. Luick, L. Sobirey, J. Siegl, T. Lompe, H. Moritz, L. W. Clark, and C. Chin, "Calibrating high intensity absorption imaging of ultracold atoms," Opt. Express **25**, 8670 (2017).
4. M. R. Andrews, D. M. Kurn, H.-J. Miesner, D. S. Durfee, C. G. Townsend, S. Inouye, and W. Ketterle, "Propagation of Sound in a Bose-Einstein Condensate," Phys. Rev. Lett. **79**, 553–556 (1997).
5. C. C. Bradley, C. A. Sackett, and R. G. Hulet, "Bose-Einstein Condensation of Lithium: Observation of Limited Condensate Number," Phys. Rev. Lett. **78**, 985–989 (1997).
6. M. Gajdacz, P. L. Pedersen, T. Mørch, A. J. Hilliard, J. J. Arlt, and J. F. Sherson, "Non-destructive Faraday imaging of dynamically controlled ultracold atoms," Rev. Sci. Instrum. **84** (2013).
7. J. M. Higbie, L. E. Sadler, S. Inouye, A. P. Chikkatur, S. R. Leslie, K. L. Moore, V. Savalli, and D. M. Stamper-Kurn, "Direct nondestructive imaging of magnetization in a spin-1 bose-einstein gas," Phys. Rev. Lett. **95**, 050401 (2005).
8. L. D. Turner, K. F. E. M. Domen, and R. E. Scholten, "Diffraction-contrast imaging of cold atoms," Phys. Rev. A **72**, 031403 (2005).

9. D. V. Freilich, D. M. Bianchi, A. M. Kaufman, T. K. Langin, and D. S. Hall, "Real-Time Dynamics of Single Vortex Lines and Vortex Dipoles in a Bose-Einstein Condensate," Sci. (80-.). **329**, 1182–1185 (2010).

10. A. Ramanathan, K. C. Wright, S. R. Muniz, M. Zelan, W. T. Hill, C. J. Lobb, K. Helmerson, W. D. Phillips, and G. K. Campbell, "Superflow in a Toroidal Bose-Einstein Condensate: An Atom Circuit with a Tunable Weak Link," Phys. Rev. Lett. **106**, 130401 (2011).

11. A. Ramanathan, S. R. Muniz, K. C. Wright, R. P. Anderson, W. D. Phillips, K. Helmerson, and G. K. Campbell, "Partial-transfer absorption imaging: A versatile technique for optimal imaging of ultracold gases," Rev. Sci. Instrum. **83**, 083119 (2012).

12. S. Serafini, M. Barbiero, M. Debortoli, S. Donadello, F. Larcher, F. Dalfovo, G. Lamporesi, and G. Ferrari, "Dynamics and Interaction of Vortex Lines in an Elongated Bose-Einstein Condensate," Phys. Rev. Lett. **115**, 170402 (2015).

13. S. Serafini, L. Galantucci, E. Iseni, T. Bienaimé, R. N. Bisset, C. F. Barenghi, F. Dalfovo, G. Lamporesi, and G. Ferrari, "Vortex Reconnections and Rebounds in Trapped Atomic Bose-Einstein Condensates," Phys. Rev. X **7**, 021031 (2017).

14. S. Serafini, "Dynamics of Vortices and their Interactions in Bose-Einstein Condensates," Phd, University of Trento (2017).

15. E. M. Seroka, A. V. Curiel, D. Trypogeorgos, N. Lundblad, and I. B. Spielman, "Repeated measurements with minimally destructive partial-transfer absorption imaging," Opt. Express **27**, 36611 (2019).

16. C. Mordini, D. Trypogeorgos, A. Farolfi, L. Wolswijk, S. Stringari, G. Lamporesi, and G. Ferrari, "Measurement of the canonical equation of state of a weakly interacting 3d bose gas," arXiv:2003.13627 (2020).

17. S. Mann, "Compositing multiple pictures of the same scene," in *Proc. IS&T Annual Meeting, 1993,* (1993), pp. 50–52.

18. G. Lamporesi, S. Donadello, S. Serafini, and G. Ferrari, "Compact high-flux source of cold sodium atoms," Rev. Sci. Instrum. **84**, 063102 (2013).

19. A. Görlitz, T. L. Gustavson, A. E. Leanhardt, R. Löw, A. P. Chikkatur, S. Gupta, S. Inouye, D. E. Pritchard, and W. Ketterle, "Sodium Bose-Einstein Condensates in the F=2 State in a Large-Volume Optical Trap," Phys. Rev. Lett. **90**, 090401 (2003).

20. M. Horikoshi, A. Ito, T. Ikemachi, Y. Aratake, M. Kuwata-Gonokami, and M. Koashi, "Appropriate Probe Condition for Absorption Imaging of Ultracold 6 Li Atoms," J. Phys. Soc. Jpn. **86**, 104301 (2017).

21. F. Dalfovo, S. Giorgini, L. P. Pitaevskii, and S. Stringari, "Theory of Bose-Einstein condensation in trapped gases," Rev. Mod. Phys. **71**, 463–512 (1999).

22. R. Grimm, M. Weidemüller, and Y. B. Ovchinnikov, "Optical Dipole Traps for Neutral Atoms," in *Advances In Atomic, Molecular, and Optical Physics,* vol. 42 B. Bederson and H. Walther, eds. (Academic Press, 2000), pp. 95–170.

23. P. B. Wigley, P. J. Everitt, K. S. Hardman, M. R. Hush, C. H. Wei, M. A. Sooriyabandara, P. Manju, J. D. Close, N. P. Robins, and C. C. N. Kuhn, "Non-destructive shadowgraph imaging of ultra-cold atoms," Opt. Lett. **41**, 4795 (2016).

24. L. Chomaz, S. Baier, D. Petter, M. J. Mark, F. Wächtler, L. Santos, and F. Ferlaino, "Quantum-fluctuation-driven crossover from a dilute bose-einstein condensate to a macrodroplet in a dipolar quantum fluid," Phys. Rev. X **6**, 041039 (2016).

25. C. R. Cabrera, L. Tanzi, J. Sanz, B. Naylor, P. Thomas, P. Cheiney, and L. Tarruell, "Quantum liquid droplets in a mixture of Bose-Einstein condensates," Science **359**, 301–304 (2018).

26. G. Semeghini, G. Ferioli, L. Masi, C. Mazzinghi, L. Wolswijk, F. Minardi, M. Modugno, G. Modugno, M. Inguscio, and M. Fattori, "Self-bound quantum droplets of atomic mixtures in free space," Phys. Rev. Lett. **120**, 235301 (2018).